

Microstructural and magnetic property of $\text{Co}_{1-x}\text{Zn}_x\text{Fe}_2\text{O}_4$ nanoparticles synthesized by the hydrothermal method

H- Y. He*

College of Materials Science and Engineering, Shaanxi University of Science and Technology, Xi'an, Shaanxi 710021, China

The cobalt zinc ferrite ($\text{Co}_{1-x}\text{Zn}_x\text{Fe}_2\text{O}_4$ $x = 0.1-1.0$) nanoparticles were synthesized by a hydrothermal method. Effects of zinc content and synthesis time on the microstructure and magnetic property of the nanoparticles were studied. The experimental results indicated that Zn^{2+} substitution for Co^{2+} and different synthesis time lead to obvious changes in microstructure and magnetic property of the ferrites. The saturation magnetization of the nanoparticles showed maximal value for the Zn content $x = 0.2$ and overall increased as increasing synthesis time from 12 hrs to 24 hrs. The residual magnetization, the coercivity and anisotropy constant had similar variation trends with shape anisotropy as varying Zn content.

Key words: Nanostructured materials, Microstructure, Optical spectroscopy, Magnetic property.

Introduction

Over recent decades, the fabrication of spinel ferrite nanoparticles has been widely investigated due to their excellent magnetic and electrical properties, and their potential uses in many areas, such as magnetic devices, recording tapes or disks, microwave absorbers, biomedical materials, and active components of ferrofluids [1-5]. Among various kinds of spinel ferrites, cobalt ferrite (CoFe_2O_4) is one of the promising hard magnetic materials having wide application [6] because of its high saturation magnetization and coercivity. However, in some practical application various magnetic properties must be tailored. Such as, in biomedical application the nanoparticles used should be magnetically in super-paramagnetic unblocked state with relatively low blocking temperature and coercivity, and in magnetostrictive application relative low saturation magnetization is required [7]. These requirements can be done by varying the size and morphology et al. of the nanoparticles or by adding the concentrations of soft (e.g. zinc ferrite) in cobalt ferrites [7].

To date, many methods have been developed to prepare spinel ferrite nanopowders, such as aerosol route [8], the co-precipitation method [7, 9], the usual ceramic technique [10], the hydrolysis method [11], the microwave-hydrothermal method [12], and the hydrothermal method [13]. The hydrothermal method is widely used because of its simple process, low cost, low synthesis temperature, and small particle size, less thermal stress, and less internal defect of synthesized powders [13].

Since the magnetic property of spinel ferrites is associated with their morphology and size, the various

applications require strict control over the morphology and size of the particles [14]. Different synthesis methods and process conditions might result in remarkable difference in microstructure and property of the nanoparticles.

In the current study, we focus on the hydrothermal synthesis of $\text{Co}_{1-x}\text{Zn}_x\text{Fe}_2\text{O}_4$ nanoparticles and examining the effect of the zinc content and synthesis time on microstructure and magnetic property of the synthesized nanoparticles.

Experimental

Cobalt chloride ($\text{CoCl}_2 \cdot 6\text{H}_2\text{O}$, Hebei Kingway Chemical Industry Co. Ltd. China), zinc nitrate ($\text{Zn}(\text{NO}_3)_2 \cdot 6\text{H}_2\text{O}$, Shenyang Hua Bai Tai Chemical Co. Ltd, China), and iron nitrate ($\text{Fe}(\text{NO}_3)_3 \cdot 9\text{H}_2\text{O}$, Beijing Baishunchem. Co. Ltd., China) were used as starting materials. The chemicals used were all analytical agent without further processing. The chemicals were weighed according to the required stoichiometric proportions of $\text{Co}_{1-x}\text{Zn}_x\text{Fe}_2\text{O}_4$ ($x = 0, 0.2, 0.4, 0.6, 0.8, \text{ and } 1.0$) and dissolved in de-ionic water with same volume of 10 ml. The concentration of Fe^{3+} in such solution was 0.04 mol l^{-1} . NaOH with double gram equivalents of all metal cations was dissolved in small amount of deionic water (5 ml) and completely dropped into the solutions with magnetic stirring. This relative large amount of NaOH addition can assure the solution $\text{pH} > 10$ throughout and so full precipitation of all cations. The precursor solutions were then transferred into autoclaves (volume: 25 ml, degree of filling: 80 vol.%) and filled to 20 ml with deionic water. After sealing, the hydrothermal reaction was then carried out in hydrothermal oven at 180°C for 12 hrs and 24 hrs, respectively. Heating rate was about $30^\circ\text{C} \cdot \text{min}^{-1}$. After natural cooling in furnace, the products were washed repeatedly with distilled water, and then dried

*Corresponding author:

Tel : +0086-15319453608

E-mail: hehy@sust.edu.cn, 917894940@qq.com

at 100 °C for 24 hrs.

The crystalline structure and phase of the synthesized $\text{Co}_{1-x}\text{Zn}_x\text{Fe}_2\text{O}_4$ nanoparticles were identified at room temperature using X-Ray diffractometer (XRD, $\text{CuK}\alpha_1$, $\lambda = 0.15406$ nm, Model No: D/Max--2200PC, Rigaku, Japan). The particle size of the nanoparticles was determined by software Jade 5 provided with the diffractometer. The morphology of the nanoparticles was analyzed using scanning electron microscopy (SEM, Model No: JXM-6700F, Japan). Fourier transform infrared spectra of the nanoparticles were measured with Fourier transform infrared spectrometer (FTIR, Model no: VERTEX 70, Bruke, German). KBr was used as matrix to disperse the ferrite powder for compressing disk sample. The magnetic property was measured with a vibrating sample magnetometer (VSM, Model No: Versa Lab, Quantun Design, USA)

Results and Discussion

XRD analysis

Fig. 1(a-b) shows the XRD patterns of the synthesized nanoparticles. All diffraction peaks are matched with standard powder diffraction data of spinel ferrites including Fe_3O_4 (JCPDS: 79-1744), CoFe_2O_4 (JCPDS: 22-1086), and ZnFe_2O_4 (JCPDS: 77-0011), indicating that the nanoparticles were composed of single phase $\text{Co}_{1-x}\text{Zn}_x\text{Fe}_2\text{O}_4$ without any other impurities. The XRD peaks enhance as increasing synthesis time, and show fluctuant changes as increase in Zn content. The average particle sizes of the

nanoparticles are determined from XRD data analysis and are in range of 9.0 ~ 15.6 nm that overall decreases and increases with increase in Zn content and synthesis time, respectively (Fig. 1(c)).

The orientation degree of the $(hk0)$ plane was calculated from Eq. (1) deduced from a formula in literature [15]

$$O_{hk0} = (I_{220} + I_{440})/I_{311} \quad (1)$$

The larger the O_{hk0} value, the larger the abundance of crystallites oriented in the $[hk0]$ direction. Similarly, O_{220} value is calculated according to:

$$O_{220} = I_{220}/I_{311} \quad (2)$$

The calculated results (Fig. 1d) indicate that the O_{hk0} value and the O_{220} value varied and have overall similar relation with Zn content, but a maximal value shifts with synthesis time. This reveals obvious anisotropy variation due to Zn^{2+} substitutions and synthesis time, and may be ascribed to the distribution variations of Zn^{2+} , Co^{2+} , and Fe^{3+} cations in A-sites and B-sites with Zn content.

SEM analysis

The morphology of the $\text{Co}_{1-x}\text{Zn}_x\text{Fe}_2\text{O}_4$ nanoparticles was determined by SEM analysis. Fig. 2 and 3 shows typical SEM micrographs of the nanoparticles synthesized for 12 hrs and 24 hrs, respectively. The particles of the nanoparticles are nearly spherical with somewhat

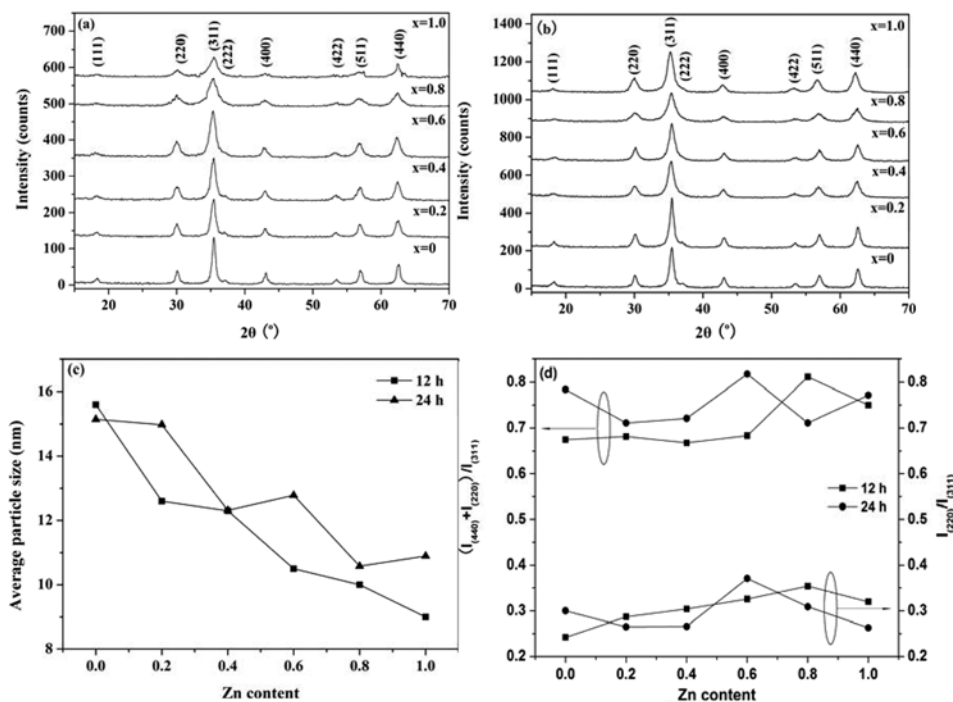


Fig. 1. XRD patterns of the $\text{Co}_{1-x}\text{Zn}_x\text{Fe}_2\text{O}_4$ nanoparticles synthesized for (a) 12 hrs and (b) 24 hrs; (c) Average particle size and (d) O_{hk0} and O_{220} of the nanoparticles determined with XRD data analysis.

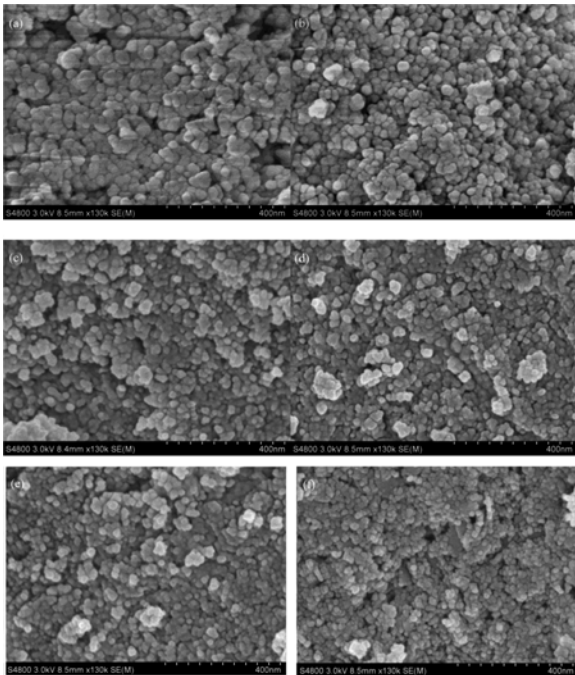


Fig. 2. SEM micrographs of the $\text{Co}_{1-x}\text{Zn}_x\text{Fe}_2\text{O}_4$ nanoparticles synthesized for 12 hrs.

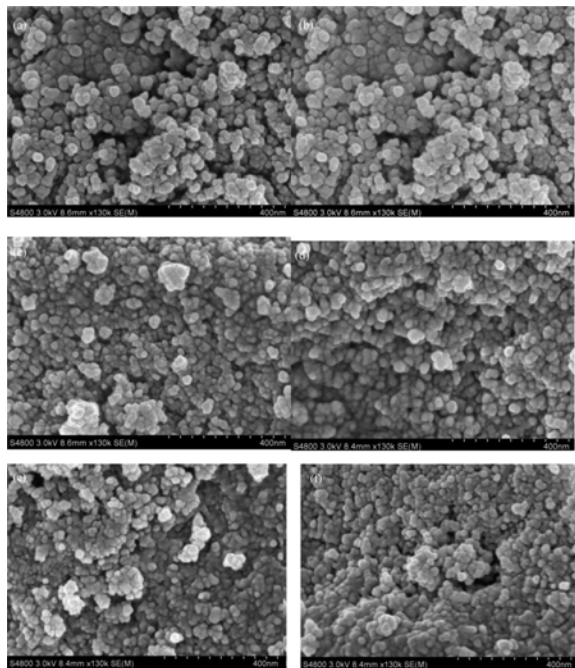


Fig. 3. SEM micrographs of the $\text{Co}_{1-x}\text{Zn}_x\text{Fe}_2\text{O}_4$ nanoparticles synthesized for 24 hrs.

agglomerate. From the SEM micrographs of the nanoparticles, the average particle sizes of the ferrite nanoparticles synthesized for 12 hrs and 24 hrs are in the ranges of $\sim 10\text{-}28$ nm and $\sim 13\text{-}32$ nm, respectively. The estimated average particle sizes decrease with increase in Zn content (x) and increase with increase in synthesis time, agreeing to the values calculated from XRD analysis.

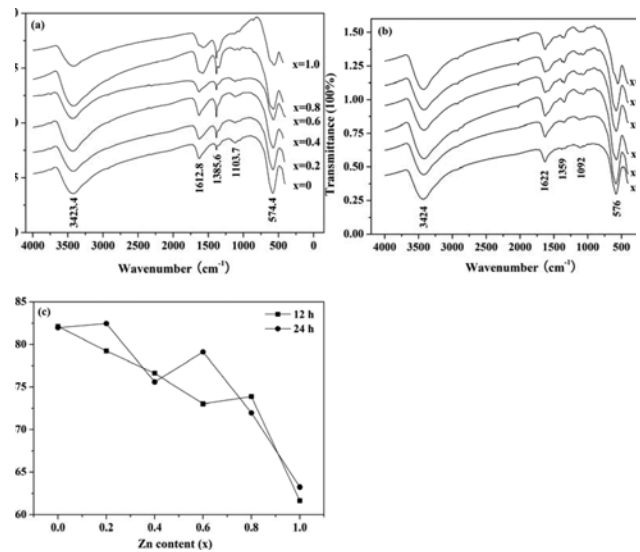


Fig. 4. FTIR spectra of the $\text{Co}_{1-x}\text{Zn}_x\text{Fe}_2\text{O}_4$ nanoparticles synthesized for (a) 12 hrs and (b) 24 hrs; (c) Positions of peaks at ~ 576 nm versus Zn content.

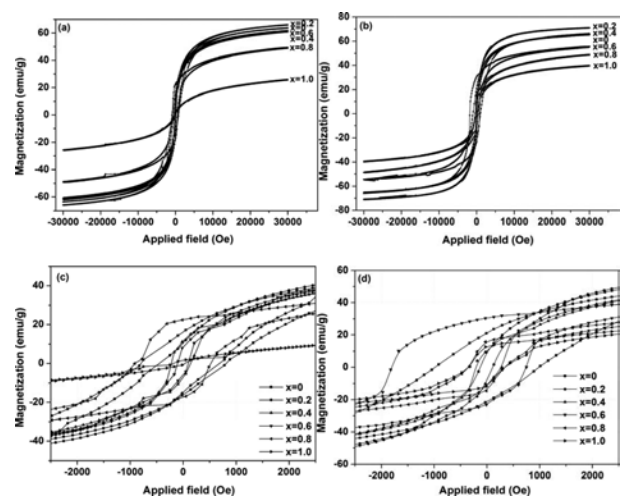


Fig. 5. Room temperature magnetic hysteresis loops of the $\text{Co}_{1-x}\text{Zn}_x\text{Fe}_2\text{O}_4$ nano-particles synthesized for (a) 12 hrs and (b) 24 hrs; Part of the curve near the origin in the (c) Fig. 6(a) and (d) Fig. 6(b).

FTIR analysis

Fig. 4(a-b) show the FTIR spectra of the nanoparticles. The broad peak observed at ~ 3424 cm^{-1} is attributed to the stretching vibration of surface hydroxyls adsorbed on surface and O-H groups in adsorbed water, which indicates the adsorbed moisture [16]. The peaks at ~ 1622 cm^{-1} and ~ 1359 cm^{-1} are assigned to H-O-H bending vibration in water molecular [17] or OH deformation vibration due to surface hydroxyls [18, 19]. The weak peak at ~ 1092 cm^{-1} could be assigned to the C-O stretching [20] due to adsorbed CO_2 . The two peaks at ~ 576 cm^{-1} and below 400 cm^{-1} are assigned as the vibration of ferrite groups [21], corresponding to the tetrahedral and octahedral sites of positive ions in the ferrite, respectively [17, 22]. The absorption peak

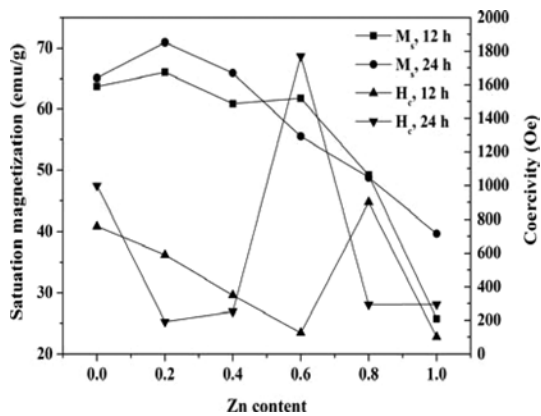


Fig. 6. Variations of saturation magnetization and coercivity of the $\text{Co}_{1-x}\text{Zn}_x\text{Fe}_2\text{O}_4$ nanoparticles with Zn content.

centered at ~ 576 nm overall shifts to low wavenumber as increase in Zn content (Fig. 4©). This can be ascribed to the increase in distance between $\text{Fe}^{3+}\text{-O}^2$ in the tetrahedral sites. This confirms the formation of $\text{Co}_{1-x}\text{Zn}_x\text{Fe}_2\text{O}_4$ structure.

Magnetic property

Fig. 5(a-b) show the room temperature hysteresis loops of the $\text{Co}_{1-x}\text{Zn}_x\text{Fe}_2\text{O}_4$ nanoparticles. With increasing applied field, the magnetization of the $\text{Co}_{1-x}\text{Zn}_x\text{Fe}_2\text{O}_4$ nanoparticles increases, and nearly reaches the saturation state under highest magnetic fields of 30 KOe. The magnetizations are more saturate for the nanoparticles synthesized for 24 hrs than 12 hrs under magnetic fields of 30 KOe. This is due to stronger effect of spin canting in the particles synthesized for 12 hrs because their larger specific area leads to more dangling bonds (uncompensated electrons) at surface of the particles. The enlargements of center part in the Fig. 6(a-b) are showed in Fig. 5(c-d), which indicates that the nanoparticles are all ferromagnetic. Maximum magnetization of the nanoparticles at applied field of 30 KOe (identified as saturation magnetization M_s) is in the range of $25.77 \sim 70.95 \text{ emu} \cdot \text{g}^{-1}$ that first increases and then overall decrease with increase of Zn content, and increase as increase in synthesis time. The ferrites with Zn content $x = 0.2$ show maximal M_s for the both synthesis times (Fig. 7(a)). This can be mainly ascribed to maximal cation distribution of Fe^{3+} and Co^{2+} at the octahedral site (B-site) at Zn content $x = 0.2$ since magnetic moments of Zn^{2+} , Co^{2+} and Fe^{3+} are $0 \mu\text{B}$, $3 \mu\text{B}$ and $5 \mu\text{B}$, respectively. Another reason may be the decrease in average particle size with increasing Zn content from $x = 0.2$ to 1.0. The similar variation in saturation magnetization with particle size come from different annealing temperature had also been reported in the literature [8]. This variation similar to smaller saturation magnetization of the nanoparticles compared to bulk material (80.5 emu g^{-1} for CoFe_2O_4 and 42.5 emu g^{-1} for ZnFe_2O_4) [20, 23-25] due to the spin

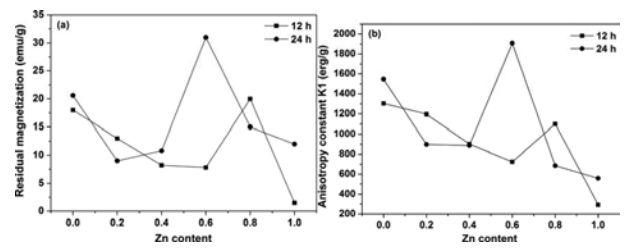


Fig. 7. (a) Residual magnetization and (b) anisotropy constant of the $\text{Co}_{1-x}\text{Zn}_x\text{Fe}_2\text{O}_4$ nanoparticles.

canting at the surface of ferrite nanoparticles [26]. The magnetic properties of the materials are generally believed to be dependent on the magnetization direction, sample shape, crystallinity, and particle size, etc. In the particle size range of $10 \sim 100$ nm, the decrease in the saturation magnetization has been explained in terms of its non-collinear spin arrangement at or near the surface of the particle. For smaller crystals the saturation magnetization generally had a value that was significantly lower than the bulk value, while larger size crystals have values approaching those of the bulk. This is attributed to the greater fraction of surface spins in the smaller crystal particles that tend to be in a canted or a spin glass-like state with a smaller net moment [27, 28]. Moreover, the saturation magnetization of the particles is not linearly decreased with increasing Zn content from $x = 0.2$ to 1.0. This can be mainly ascribed to nonlinear variation of cation distribution and particle size. In addition, the shape anisotropy is the dominant form of anisotropy, being more important than magnetocrystalline anisotropy, as particle size is smaller than $20 \mu\text{m}$ [29]. Since the easy magnetization direction of CoFe_2O_4 is in a-axis, the saturation magnetization of the particles could also be associated with their shape anisotropy (O_{hk0} and O_{220}) [17].

Fig. 6 also shows the coercivity (H_c) of the nanoparticles with various Zn contents. They are in the range of $0.125 \sim 1.77$ kOe and overall decrease with increase in Zn content, but an unusual large maximal value appears at Zn content $x = 0.6$ and 0.8 for the synthesis time of 12 hrs and 24 hrs, respectively. Usually, the H_c of the $\text{Co}_{1-x}\text{Zn}_x\text{Fe}_2\text{O}_4$ nanoparticles decreases or linearly decreases with increasing Zn content [30, 31], or show maximal value at Zn content at which the saturation magnetization is also largest [32].

This trend may be attributed to the lower magnetocrystalline anisotropy of Zn^{2+} as compared to that of Co^{2+} ions which leads to lower coercivity according to the Stoner-Wolfarth model for nanoparticles ($H_c = 2K_1/\mu_0 M_s$) [33]. Anisotropy constant (K_1) of the CoFe_2O_4 and the ZnFe_2O_4 is $\sim 2 \times 10^6 \text{ erg/cm}^3$ [34] and less than absolute value of $-1 \times 10^4 \text{ erg/cm}^3$ [34], respectively. The negative K_1 value of the ZnFe_2O_4 expresses an axis of easy magnetization preferring to (111) direction, being different from (100) direction for the

positive K_1 value. Since the magnetic property of the nanoparticles is associated not only with intrinsic magneto-crystalline anisotropy but also more importantly with shape anisotropy, the variation of the coercivity with zinc content could also be associated with the (hk0)-orientation degree (O_{hk0} and O_{220}) (Fig. 1d). It can be found that the usually large maximal values in coercivity appear at same Zn content $x = 0.6$ and 0.8 for the synthesis times of 12 hrs and 24 hrs, respectively. The nanoparticles with these Zn contents also show largest the (hk0)-orientation degree (O_{hk0} and O_{220}). This might imply that the axes of easy magnetization of the ferrites have shifted from (100) to (111). In addition, the coercivity (H_c) is probably also sensitive to porosity and grain size [35]. The decreases in coercivity with increase in Zn content may be attributed to their decreases in particle size to some extent. This is because coercivity increases with increase in particle size when particle size is smaller than single-domain size (40 nm [36]). Maximal coercivity of CoFe_2O_4 , $\text{Co}_{0.4}\text{Zn}_{0.6}\text{Fe}_2\text{O}_4$ and ZnFe_2O_4 particles appeared at critical particle size of ~ 40 nm [8]. Bulk CoFe_2O_4 materials sintered at different temperatures showed also maximal coercivity at critical particle size of ~ 40 nm [37]. Thus, the size (~ 40 nm) can be further verified as the single-domain sizes of these ferrites.

The anisotropy constant of the nanoparticles is calculated with Stoner Wolfarth model for nanoparticles [33]:

$$K_1 = \frac{1}{2} \mu_0 H_c M_s \quad (3)$$

where μ_0 is vacuum permeability, $\mu_0 = 1$ in system of egs unit. Calculated anisotropy constant together with residual magnetization of the nanoparticles with varying Zn contents are showed in Fig. 7a and 7b, respectively. The residual magnetizations (M_r) of the nanoparticles are in the range of ~ 1.5 -20.6 emu/g. The anisotropy constants (K_1) are in the range of ~ 196.1 -1907.5 erg/g. The M_r and K_1 vary consistently with (hk0)-orientation degree (O_{hk0} and O_{220}) as increasing Zn content.

Conclusions

$\text{Co}_{1-x}\text{Zn}_x\text{Fe}_2\text{O}_4$ ($x = 0.1$ -1.0) ferrites were synthesized using a hydrothermal method. The room temperature X-ray diffraction confirms the formation of single-phase Co-Zn ferrites at 180 °C for 12 hrs and 24 hrs. The average particle sizes determined with analyses of XRD data and SEM are found to be in the range of ~ 8.5 -15.9 nm and ~ 10 -32 nm, respectively, and decrease and increase with increase in Zn content and synthesis time, respectively. The room temperature VSM results show that the $\text{Co}_{1-x}\text{Zn}_x\text{Fe}_2\text{O}_4$ nanoparticles exhibit ferromagnetic behavior. The saturation magnetization of the particles shows maximal value as Zn content is 0.2 for both synthesis times of 12 hrs and 24 hrs due to preferential occupation of A-sites by Zn^{2+} leading to

magnetic Fe^{3+} and Co^{2+} cations shift to B-sites. The coercivities overall decrease with increase in Zn content, but show an unusual large maximal value at Zn content $x = 0.6$ and 0.8 for synthesis time of 12 hrs and 24 hrs, respectively. These maximal coercivities might be due to large (hk0)-orientation degrees and transformations in axes of easy magnetization from (100) to (111) with Zn substitution. The residual magnetization and anisotropy constant vary consistently with (hk0)-orientation degree.

Acknowledgments

The authors thank the Ms. Chen of the Shaanxi University of Science and Technology for her kind assistance in SEM measurement and Mr. F.-X. Yan of the Advanced Material Analysis and Test Center of the Xi'an University of Technology for his kind assistance in magnetic property measurement.

References

1. M. Kaiser, J. Alloys Compd. 468 (2009) 15-21.
2. M.J. Iqbal, M.R. Siddiquah, J. Alloys Compd. 453 (2008) 513-518.
3. M. Srivastava, A.K. Ojha, S. Chaubey, A. Materny, J. Alloys Compd. 481 (2009) 515-519.
4. I.H. Gul, A. Maqsood, J. Alloys Compd. 465 (2008) 227-231.
5. Y. Köseođlu, A. Baykal, M.S. Toprak, F. Gözüak, A.C. Basaran, B. Akas, J. Alloys Compd. 462 (2008) 209-213.
6. X. Meng, H. Li, J. Chen, L. Mei, K. Wang, X. Li, J. Magn. Mater. 321 (2009) 1155-1158.
7. V.L. Mathe, A.D. Sheikh, Physica B 405 (2010) 3594-3598
8. S. Singhal, J. Singh, S.K. Barthwal, K. Chandra. J. Solid State Chem. 178 (2005) 3183-3189.
9. R. Arulmurugan, G. Vaidyanathan, S. Sendhilnathan, B. Jeyadevan, J. Magn. Mater. 303 (2006) 131-137.
10. A. Tawfik, I.M. Hamada, O.M. Hameda, J. Magn. Mater. 250 (2002) 77-82.
11. G.V. Duong, N. Hanh, D.V. Linh, R. Groessinger, P. Weinberger, E. Schafner, M. Zehetbauer, J. Magn. Mater. 311 (2007) 46-50.
12. C.-K. Kim, J.-H. Lee, S. Katoh, R. Murakami, M. Yoshimura, Mater. Res. Bull. 36 (2001) 2241-2250.
13. F. Gözüak, Y. Köseođlu, A. Baykal, H. Kavas, J. Magn. Mater. 321 (2009) 2170-2177.
14. G.V. Kurlyandskaya, J. Cunanan, S. M. Bhagat, J. C. Apesteguy, S. E. Jacobo, J. Phys. Chem. Solids 68 (2007) 1527-1532.
15. W. Schwartz, P. G. Clem, J. A. Voigt, E. R. Byhoff, M. V. Stry, T. J. Headley, N. A. Missert, J. Am. Ceram. Soc. 82[9] (1999) 2359-2367.
16. R. Mukherjee, T. Sahu, S. Sen, P. Sahu, Mater. Chem. Phys. 128 (2011) 365-370.
17. M. Srivastava, S. Chaubey, A.K. Ojha, Mater. Chem. Phys. 118 (2009) 174-180.
18. E. Eloska, W. Wolski, Phys. Stat. Solidi A [132] (1992) K51-K56.
19. B.P. Ladgaonkar, A.S. Vaingankar, Mater. Chem. Phys. 56 (1998) 280- 283.
20. M.J. Buerger, Crystal Structure Analysis, Wiley

- Interscience, New York, 1960, pp. 35.
21. A.B. Nawale, N.S. Kanhe, K.R. Patil, S.V. Bhoraskar, V.L. Mathe, A.K. Das, *J. Alloys Compd.* 509 (2011) 4404-4413
 22. V. Sepelak, K. Tkacova, V.V. Boldyrev, S. Wibmann, K.D. Becker, *Physica B* 234-236 (1997) 617-619.
 23. Y. Shi, J. Ding, H. Yin, *J. Alloys Compd.* 308 (2000) 290-295.
 24. R. Valenzuela, *Magnetic Ceramics*, Cambridge University Press, Cambridge, 1994.
 25. J. Jiang, Y.M. Yang, *Mater. Lett.* 61 (2007) 4276-4279.
 26. N. Bao, L. Shen, Y. Wang, P. Padhan, A. Gupta, *J. Am. Chem. Soc.* 129 (2007) 12374-12375.
 27. M. George, A.M. John, S.S. Nair, P.A. Joy, M.R. Nantharaman, *J. Magn. Mater.* 302 (2006) 190-195.
 28. R.H. Kodama, A.E. Berkowitz, *Phys. Rev. B* 59 (1999) 6321-6336.
 29. Bruce M. Moskowitz, *Hitchhiker's Guide to Magnetism*, http://www.irm.umn.edu/hg2m/hg2m_c/hg2m_c.html.
 30. H. Sozeri, Z. Durmus, A. Baykal. *Mater. Res. Bull.* 47[9] (2012) 2442-2448.
 31. K.H. Maria, S. Choudhury and M.A. Hakim. *International Nano Letters* 3 (2013) 42.
 32. R. Rani, S.K. Sharma, K.R. Pirola, M. Knobel, S. Thakur and M. Singh. *Ceram. Int.* 38[3] (2012) 2389-2394.
 33. E.C. Stoner, E.P. Wohlfarth, *Phil. Tans. Roy. Soc. A240* (1948) 599-642, reprinted in *IEEE Trans. Magn.* 27 (1991) 3475-3478.
 34. M.H. Servits, J.H. Saunders, *Phys. Rev.* 102 (1956) 366-367.
 35. K. Maaz, S. Karim, A. Mashiatullah, J. Liu, M.D. Hou, Y.M. Sun, J.L. Duan, H.J. Yao, D. Mo, Y.F. Chen, *Physica B* 404 (2009) 3947-3951.
 36. J.H. Yin, J. Ding, B.H. Liu, X.S. Miao, J.S. Chen, *J. Magn. Mater.* 310 (2007) 2537-3539.
 37. S. Imine, F. Schoenstein, S. Merccone, M. Zaghrioui, N. Bettahar, N. Jouini, *J. Euro. Ceram. Soc.* 31 (2011) 2943-2955.